THE ASTROPHYSICAL JOURNAL, 438:708–718, 1995 January 10

INTERSTELLAR SCATTERING TOWARD CYGNUS X-3: MEASUREMENTS OF ANISOTROPY AND OF THE INNER SCALE

L. A. MOLNAR AND R. L. MUTEL
Department of Physics and Astronomy, University of Iowa, Iowa City, IA 52242
M. J. REID
Harvard-Smithsonian Center for Astrophysics, 60 Garden Street, Cambridge, MA 02138
AND
K. J. JOHNSTON
Naval Research Laboratory, Code 4130, Washington, DC 20375
Received 1990 January 8; accepted 1993 June 18

ABSTRACT

We present 18 cm wavelength VLBI observations of Cyg X-3 obtained 1989 June 6 along with 18 and 20 cm VLA A-array data obtained 1985 February 8. In both data sets, the flux density was relatively high, and the intrinsic source size small compared to the scattering, ideal conditions for a detailed study of interstellar scattering. We find that the scattering disk is anisotropic, with an axial ratio 1.31 ± 0.02 along position angle $52\overset{\circ}{.}0 \pm 1\overset{\circ}{.}5$. This is the first unambiguous measurement of anisotropic scattering in the interstellar medium. We also find a significant break in the phase structure function, the first measurement of a break in any source. The data exclude a steep turbulent spectrum, but are consistent with a shallow turbulent spectrum with an inner scale of 300 km, with a net uncertainty of $\sim 50\%$.

We tentatively identify the scattering plasma with the H II region DR 11, for which we estimate a visual extinction of 4 mag, and an emission measure toward Cyg X-3 of 6000 cm^{-6} pc. We make the case that DR 11 is part of a shell of H II regions centered on the Cyg OB2 association (which is ~ 1.8 kpc distant) that is 2° (60 pc) in radius and expanding at 10 $\mathrm{km\ s}^{-1}$. Our inner scale is consistent with that expected for an H II region, and the amount of scattering is consistent with the emission measure. We discuss how the anisotropy can be used to confirm the identification with DR 11 and to distinguish between different models of turbulence by comparison with measurements of the polarization of starlight along the line of sight.

Subject headings: H II regions — open clusters and associations: individual (Cygnus OB2) — polarization — radio continuum: stars — stars: individual (Cygnus X-3)

1. INTRODUCTION

While the phenomenon of interstellar scattering (ISS) is well established, it remains to measure the details of the turbulent spectrum, determine in which phase(s) of the interstellar medium the scattering occurs, and what mechanisms determine the turbulent spectrum. Interferometry may be used to measure the phase structure function as a function of baseline, which is a simple transform of the turbulent spectrum. Until now the power-law dependence of the structure function on baseline has only been well determined in a few cases, and in no single case has it been measured well enough over a sufficiently large range of baselines to see significant change in slope with baseline.

Anderson et al. (1972) were the first to notice the large amount of ISS of Cyg X-3 in 408 MHz data obtained at Jodrell Bank. Their results have been confirmed by a number of observers out to frequencies as high as 22 GHz (Molnar, Reid, & Grindlay 1988 and references therein). Cyg X-3 occasionally has large flares at radio frequencies, and in the first few days of one of these flares, ISS measurements of Cyg X-3 have a *combination* of advantages shared by no other source: (1) intrinsic size much less than scattering size for frequencies less than 5 GHz, (2) flux densities of 3–20 Jy from 0.3–30 GHz, (3) measurable scattering on baselines from 10–1000 km, (4) no limitations from confusion sources in this range of baselines and frequencies, and (5) a comparison source (2005+403) that is nearby (2°.4), compact, and has similar flux density (~4 Jy) in this range of baselines and frequencies, which can therefore be used for unusually high accuracy calibration of visibility amplitudes. In this paper we present observations of Cyg X-3 taken during two such epochs and discuss their implications for models of scattering.

In § 2, we present VLA and VLBI observations, the calibration procedures, and preliminary modeling with an anisotropic power law structure function. In § 3 we analyse the combined data sets in terms of a broken power-law model (§ 3.1) and a Kolmogorov model with an inner scale (§ 3.2). In § 3.3 we compare these results to previous observations. In § 4 we discuss in some detail the implications for models of turbulent scattering of our observation of anisotropic scattering and of the inner scale. In particular we explore the possibility that the scattering is largely produced in an H II region in the line of sight.

2. THE OBSERVATIONS

2.1. *Very Long Baseline Interferometry*

We observed Cyg X-3 on 1989 June 6 from 4:00 to 5:30 UT at 1665 MHz with a 2 MHz bandwidth using MkII recording terminals (detecting IEEE left circular polarization) at the Very Long Baseline Array[1] (VLBA) antenna on Kitt Peak and at the Very Large Array (VLA).[1] We alternated making 5 minute

[1] The VLA and the VLBA are facilities of the National Radio Astronomy Observatory which is operated by Associated Universities Inc., under contract with the National Science Foundation.

scans of Cyg X-3 and 5 minute scans of the nearby source 2005+403, recording a total of eight pairs of scans. We also recorded the correlations of the individual VLA antennas with each other, using a 50 MHz bandwidth. For an optimum VLBI SNR we "phased" and summed together the signals of all 27 VLA antennas. The VLA was in the C-configuration, with maximum spacing of ~3 km. At these spacings both sources are unresolved, so that we could continually phase the array for each source while the VLBI data were being recorded.

The VLBA antenna at Kitt Peak offered a new opportunity to measure scattering on baselines of a few hundred kilometers. In choosing the observing frequency, we went as low as possible both to make interstellar scattering a strong effect as well as to make intrinsic source structure a small effect, and yet not so low as to have scattering make the visibilities undetectable. Based on previous measurements of scattering in Cyg X-3 (Molnar et al. 1988 and references therein), we estimated that we could confidently detect 1665 MHz visibilities ($\gamma > 0.1$) on the Kitt Peak–VLA baseline for the first 1.5 hr of mutual visibility. Because of the large baseline foreshortening, we also cover a factor of 2 in baseline length during this time (100–200 km). We plot the observed (u, v) track in Figure 1.

Our observations took place only 5 days after the beginning of the first giant radio flare of Cyg X-3 to occur since 1985 December (see Waltman, Fiedler, & Johnston 1989). We chose this time to exploit several advantages. First, the flux density of Cyg X-3 was ~3 Jy during our experiment, 30 times greater than typical flux densities, allowing very high signal-to-noise measurements with the MkII VLBI system. Second, because of the long interval since the previous giant flare, we do not expect significant spatially extended flux from that flare. Finally, because of the short amount of time since the beginning of the current flare, we do not expect its size to be large enough yet to influence our visibilities. Specifically, previous measurements of the radio jets of Cyg X-3 are all consistent with expansion in the north-south direction at a rate of ~10 mas day^{-1} (Molnar et al. 1988 and references therein). The range of projected north-south baselines in our experiment was 77–106 km. Hence after 5 days we expect the source to be resolved on our baselines by only 4%–7% due to intrinsic source structure. Given that some fraction of the flux density we observed is from subsequent injections of material into the jet between flare onset near June 1 and June 6, and hence is very compact, these numbers are an upper limit to the effect we expect.

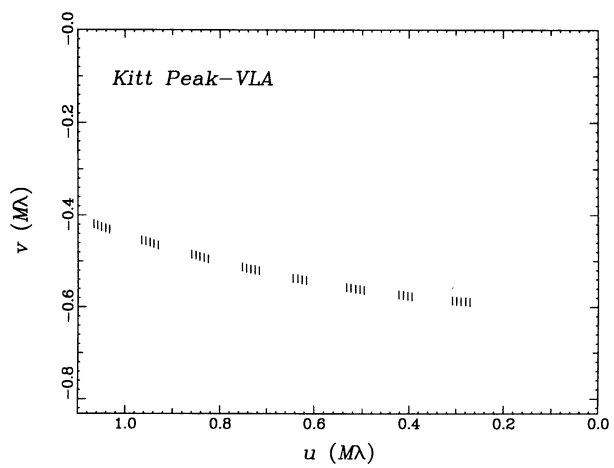

FIG. 1.—The (u, v) track in units of millions of wavelengths of the Kitt Peak–VLA baseline for the 1989 June 6 data.

2.2.1. *Calibration Procedure*

The strength of our conclusions depends on being able to convert the measured correlation coefficients into well-calibrated visibilities. By observing the comparison source 2005+403 at frequent intervals, we were able to calibrate the visibility amplitudes more accurately than is typically possible in a one-baseline experiment. As our calibration procedure differs somewhat from that most often used, we describe it in some detail.

The MkII tapes were correlated with the Block II VLBI processor at Caltech. We loaded the 2 s correlation coefficients into the Astronomical Image Processing System (AIPS), edited out data with low amplitudes (recorded while the telescopes were still slewing), and determined interferometer phase rates and group delays with the program CALIB. Then we coherently averaged the data into 1 minute bins.

The visibility of source i at time t, $\gamma_i(t)$, is related to the observed correlation coefficient, $r_i(t)$, by the expression

$$\gamma_i(t) = C_1 T_a(t)^{1/2} T_b(t)^{1/2} S_i(t)^{-1} r_i(t) , \quad (1)$$

where T_a is the system temperature of antenna a (which in this experiment is the phased VLA), T_b is the system temperature of antenna b (Kitt Peak), and S_i is the flux density of source i. C_1 includes all constant or elevation-dependent factors such as the antenna gains, digital losses, local oscillator losses, atmospheric transparency, uncertainty in the temperature of the calibration noise source and hence in the system temperature scale, and the data duty cycle at the VLA. We will set the source subscript i to A for Cyg X-3 and B for 2005+403.

Our strategy for obtaining a well-calibrated data set is to use comparisons with the nearby quasar 2005+403 to directly determine C_1 rather than to estimate the many individual factors separately. We use a priori information to determine $\gamma_B(t)$ and $S_B(t)$. Previous observations of 2005+403 reported in Molnar et al. (1984, 1985, 1988) indicate no evidence of flux density variations on the time scale of hours. The absolute flux density of 2005+403 will cancel out of our final equation, but a typical 18 cm flux density is ~3 Jy. VLBI observations (Mutel & Lestrade 1990) show the spatial structure we observe should be dominated by a 28.8 ± 0.9 mas FWHM scattering disk. On the baselines observed here this implies the source is resolved from 4% to 12%. The uncertainty in the scattering size corresponds to an uncertainty on $\gamma_B(t)$ of only 1%.

The quantity T_b is directly measured every 2 minutes. The quantity T_a refers to an average over all of the elements of the VLA. We obtain T_a to within a scale factor, C_2, by computing the amplitude, $A_i(t)$, of the vector average of the correlations of the individual VLA antennas with each other:

$$T_a(t) = C_2 S_i(t) A_i(t)^{-1} . \quad (2)$$

Note that when recording VLBI data T_{sys} corrections are not applied to the VLA correlations as they otherwise would be.

We can now write an expression for the visibility of Cyg X-3 entirely in terms of measured quantities:

$$\gamma_A(t) = C_3^{-1} A_A(t)^{-1/2} T_b(t)^{1/2} \left(\frac{S_A(t)}{S_B} \right)^{-1/2} r_A(t) , \quad (3)$$

where the effective gain

$$C_3 \equiv C_1^{-1} C_2^{-1/2} S_B^{1/2} = \gamma_B(t)^{-1} T_b(t)^{1/2} A_B(t)^{1/2} r_B(t) . \quad (4)$$

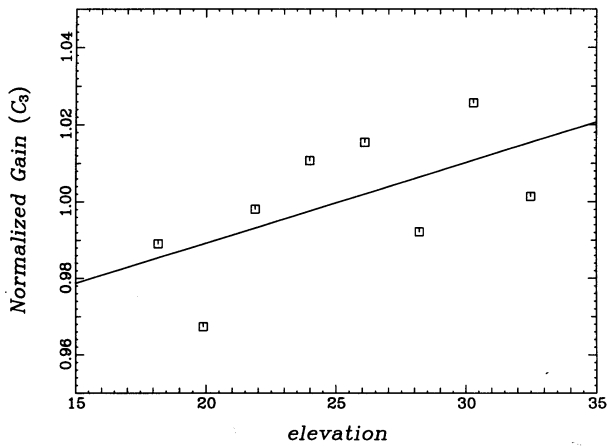

FIG. 2.—Normalized gain vs. interferometer elevation for the 2005+403 scans. The solid line is a linear fit to the data.

To calculate C_3 we compute the ratio $r_B(t)/\gamma_b(t)$ for each 1 minute record, average the results for each 5 minute scan, and then multiply by scan averages of $T_b(t)^{1/2}$ and $A_B(T)^{-1/2}$. We plot the resulting eight values, normalized to a mean of unity, as a function of interferometer elevation in Figure 2, along with a straight-line fit. The fit indicates a change in the gain of 3% over the entire range of elevation, lower at the lower elevations as expected. The rms of the data around the fit is 1.5% and is a good indication of the net uncertainty of the calibration of any single scan.

The ratio $S_A(t)/S_B$ may be determined from the VLA correlations. We apply equation (2) to the 2005+403 data to obtain eight estimates of $C_2 S_B$. For this we require $T_a(t)$ appropriately averaged over the entire array. We construct this by taking values measured for antenna 23, and weighting them according to the gain of antenna 23 relative to the average gain of the other 26 antennas as determined by the AIPS program CALIB for each scan. We then apply equation (2) to the Cyg X-3 data, using the mean of our estimates for $C_2 S_B$. We plot the resulting eight values S_A/S_B versus UT in Figure 3. The figure shows no significant evidence of time variability of Cyg X-3; the data have an rms of 0.5% around their mean value of 1.082, a greater rms than expected from radiometer noise alone, but consistent with a number of systematic effects.

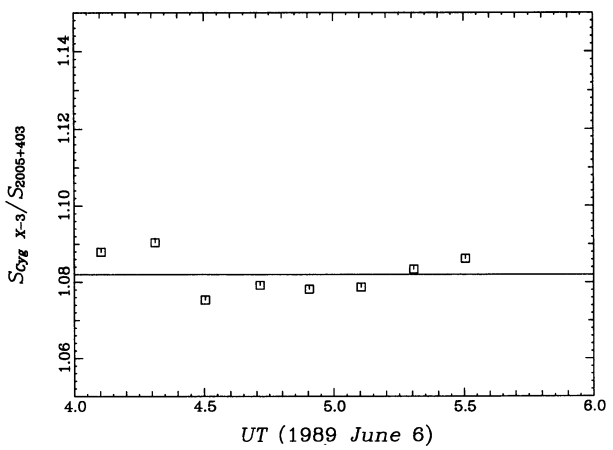

FIG. 3.—Ratio of the flux density of Cyg X-3 to that of 2005+403 vs. UT. The solid line denotes the mean of the data.

2.1.2. *Modeling of VLBI Data*

We fit our calibrated data set to an anisotropic scattering model. Following Narayan & Hubbard (1988), we assume the power spectrum of electron density turbulence to have a power-law form

$$Q(q_x, q_y) = C_N^2(\rho^2 q_x^2 + q_y^2)^{-\beta/2} = C_N^2 q_s^{-\beta}, \quad (5)$$

where q_x and q_y are spatial wavenumbers in perpendicular orientations, β is the spectral index, ρ, which we always take greater than unity, is the axial ratio of the anisotropy, and q_s is a scaled spatial wavenumber defined by the equality. The interferometer visibility is a measure of the phase structure function, $D_\phi(b_s)$, which for shallow spectra ($2 < \beta < 4$) can be written as

$$\gamma(x, y) = \exp\left[-\frac{D_\phi(b_s)}{2}\right] = \exp\left[-\ln 2\left(\frac{\pi\theta_0}{2\ln 2}\right)^{\beta-2}\left(\frac{b_s(x, y)}{\lambda_0}\right)^{\beta-2}\left(\frac{\lambda}{\lambda_0}\right)^2\right], \quad (6)$$

where λ is the observing wavelength and θ_0 is a measure of the angular size (in radians) of the scattering disk at reference wavelength λ_0 or corresponding frequency ν_0 (precisely the FWHM of the major axis for $\beta = 4$, the Gaussian case). The variable b_s is the scaled baseline length defined by

$$b_s \equiv \lambda\left(\frac{x^2}{\rho^2} + y^2\right)^{1/2}, \quad (7)$$

where x and y are the projected baselines in wavelengths in the x and y directions. We can relate x and y to u and v by

$$x = u\cos\chi - v\sin\chi; \quad y = u\sin\chi + v\cos\chi, \quad (8)$$

where χ is the position angle measured east of north of the y-axis, the major axis of the scattering disk. For the cases of steep spectra of density turbulence ($\beta > 4$), shallow spectra measured on baselines much shorter than the inner scale of turbulence, or Gaussian spectra, the expression for ensemble average visibility is that of equation (6) with β set to 4.0.

Given our limited coverage of the (u, v) plane, β is highly correlated with ρ. Therefore to get preliminary parameter estimates, we fix β to be 3.88, the value reported by Wilkinson, Spencer, & Nelson (1988). We perform a least-squares fit for ρ, χ, and θ_0, calculating uncertainties on individual data by combining in quadrature the statistical error or the correlation coefficient with a 2% random error in calibration. In Figure 4 we mark our best fit for the VLBI data in the axial ratio (ρ) versus position angle (χ) plane along with 1 to 3 σ contours around it, using the procedire of Avni (1976) to compute the contours. The minimum χ^2 provides a good fit to the data: 4.60 with 5 degrees of freedom. (The probability of exceeding this χ^2 given the validity of the model is 0.47.) By contrast a circularly symmetric fit is very unlikely: χ^2 of 51.0 with 7 degrees of freedom (a probability of 9.4×10^{-9}). Increasing the value of β to 4.0 allows a better, but still unacceptable fit to a circular model: χ^2 of 24.6 (probability of 9.0×10^{-4} or 3.3 σ). As there is no spectrum of density fluctuations that corresponds to a value of β in equation (6) greater than 4.0, we conclude that a circular model is unacceptable for any power law or Gaussian spectrum of turbulence. This is the first evidence for anisotropic scattering in Cyg X-3.

There are several checks for our interpretation of source elongation as being due to anisotropic scattering. As can be seen in Figure 4, while the precise position angle of the major

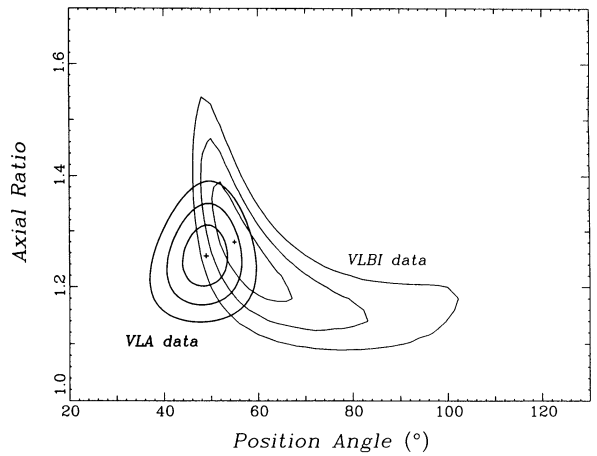

FIG. 4.—Axial ratio vs. the position angle of the major axis of the anisotropic scattering models. A cross marks the best-fit values. Solid curves denote 1 through 3 σ error contours. The fit to the 1989 June 6 VLBI data (assuming $\beta = 3.88$) is marked with normal weight lines. The fit to the 1985 February 8 VLA data (assuming $\beta = 4.00$) is marked with bold lines.

axis is correlated with the axial ratio, there is no acceptable value near 0°, the orientation always found for the radio jet (Molnar et al. 1988). This suggests that the elongation cannot be due to the intrinsic struacture of the radio jet. Also the geometric mean of the major and minor axes, 162 mas, is consistent with the size extrapolated from Wilkinson et al. (1988): 156 ± 7 mas, whereas one would expect a large size if intrinsic source structure were important. Finally, to test our sensitivity to calibrate errors we tried to force a circular fit by increasing the calibrated visibilities by an arbitrary percentage. (We plot the visibilities as a function of scaled baseline (b_s) in Figure 5 using the scaling determined in § 3.2 from a fit to the combined VLA and VLBI data sets.) We found this could only be done by adding 25%, although this contradicts the consistency in the scattering size. This value is much greater than the uncertainties derived above from the intrinsic structure of Cyg X-3 or error in the scattering size of 2005+403, and it is much greater than the 2% variation observed in the calibrated 2005+403 data.

2.2. *Very Large Array*

It is instructive to compare the VLBI data presented in the last section to VLA data obtained in the A-array (which has

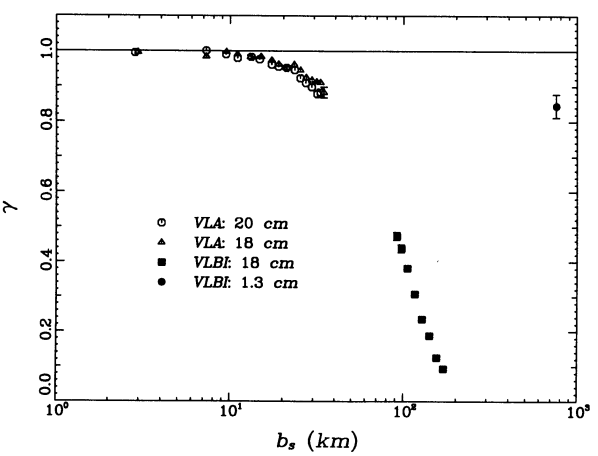

FIG. 5.—Interferometer visibility vs. baseline length, scaled for $(\rho, \chi) = (1\overset{\circ}{.}31, 52\overset{\circ}{.}0)$. Error bars are marked when larger than the symbol.

baselines as long as ~35 km) for several reasons. First, VLA data have much more complete coverage of (u, v) position angle, which allows an independent determination of the axial ratio, ρ, and orientation, χ, of the scattering disk without these parameters being correlated with each other or with other parameters. Also, VLA data may be compared with the VLBI data for evidence of time variability of the scattering disk. Finally, VLA data taken close enough in time to avoid variability may be combined with the VLBI data to study the power-law index of density fluctuations, β, over more than a decade in baseline length.

Molnar et al. (1988) presented A-array data taken at 1452 and 1652 MHz of 1985 February 8. Only 7 of the 27 antennas were used: the outermost antenna on the north arm, the outermost two on the west arm, and the second, third, eighth, and ninth antennas on the east arm. (The design of the VLA is described by Napier, Thompson, & Ekers 1983.) This data set was taken within 2 days of a several Jansky flare, the largest since 1983 October (Johnston et al. 1986). So, like the VLBI data described above, it is well suited for a high-sensitivity study of interstellar scattering undisturbed by intrinsic source structure.

Molnar et al. (1988) reported that the 20 cm data are consistent with a circular Gaussian with FWHM 229 ± 5 mas, with no limit on the ellipticity given. In that paper we tested consistency with a circular Gaussian only by a visual inspection of finely binned visibilities at various (u, v) position angles, and would not have been able to distinguish axial ratios less than 1.5 from unity. We reanalyzed these data using the technique described in § 2.1.2, performing a least-squares fit in the (u, v) plane to the elliptical scattering model described by equation (6). As in the 1988 paper, the amplitudes of the antenna gains were calibrated with measurements of 2005+403, which is well modeled as a point source on these spacings, and the phases were self-calibrated. No spacings less than 10,100 wavelengths were used, to avoid interference from large scale confusion sources.

In addition to our four model parameters (β, ρ, χ, and θ_0) we must also solve for $S(t)$ at each wavelength. Specifically we solve for 10 flux densities at 1452 MHz and 13 flux densities at 1652 MHz, one for each 2 minute scan. It is essential that this be done as accurately as possible, as we expect scattering to be a 12% effect on the longest baselines, and only a 1% effect on 10 km baselines. To simplify the software, we take an iterative approach to finding $S(t)$. We compute a light curve using all of the VLA data, correcting the measurements for an initial guess about the scattering. We compute visibilities by dividing through by the light curve. We bin the visibilities into a two-dimensional grid with 20 (u, v) position angle bins and 20 (u, v) distance bins (each 10,100 wavelengths in size), weighting each datum by the source flux density at that time. Then we perform a least-squares fit to the binned data for scattering parameters, using the same program used to fit the VLBI data. Finally, we iterate using the new fit as our input model. Using the circular Gaussian fit to the 1988 analysis as the initial guess, the first fit computed was within 1 σ of the final fit in individual solutions for both the 1452 and 1652 MHz data, which demonstrates the robustness of the iterative technique. The final uncertainties on each value of $S(t)$ were ~0.3%.

To determine the goodness of our fit, we need to know the uncertainty on individual measurements. Expected system noise at the VLA corresponds to 15 mJy for a single 30 s record with a 25 MHz bandwidth, and averaging left and right circu-

lar polarizations together. Other effects, such as correlator-based errors, may raise this value slightly for a strong source. Fitting each wavelength separately, we find a reduced χ^2 of unity corresponds to an uncertainty on an individual measurement of 24 mJy at 1452 MHz and 20 mJy at 1652 MHz. The residuals in the (u, v) plane show no systematic effects. We conclude that the data are well fitted by the model. For computing uncertainties on model parameters below, we will assume 24 and 20 mJy to be the measurement uncertainty for data at 1452 and 1652 MHz, respectively. With this assumption, we find the individual fits to the 1452 and 1652 MHz data to be consistent with each other to within 1 σ. Each fit is also inconsistent with circular symmetry at the 5 σ level, in confirmation of the VLBI analysis.

We illustrate the fit of the VLA data to an elliptical model by binning the data in two 45° wedges of the (u, v) plane centered on the major and minor axes. We plot these binned visibilities versus baseline in wavelengths along with dashed lines showing the expected visibilities along the major and minor axes for the 20 cm data in Figure 6. We plot the 18 cm data in the same manner in Figure 7. For both model curves, we use the best fit to the combined VLA described below and shown in Figure 4. The differences between the major and minor axis models are greater than 2 σ for baselines greater than 80 kλ in both figures, and all of the major axis data in this range fall below the corresponding minor axis data as expected for ellipticity.

Given consistency with expected noise estimates and between the two frequency bands, we now compute a fit to both data sets combined. We find β to be 4.07 $\pm$ 0.09. This is 2 σ from the value found by Wilkinson et al. (1988). We note again that a value of β greater than 4.0 in equation (6) has no physical correspondence in the turbulent power spectrum, but also that our fit is within 1 σ of 4.0, the value expected for baselines much shorter than the inner scale of turbulence. This is consistent with the A-array measurements of Moran et al. (1990) of NGC 6334B, from which they derived $\beta = 4.01 \pm 0.02$.

We compute a best-fit model fixing β to be 4.0, and mark the best fit along with 1 to 3 σ contours with bold lines in Figure 4 for comparison with the VLBI fit. The two fits agree to within

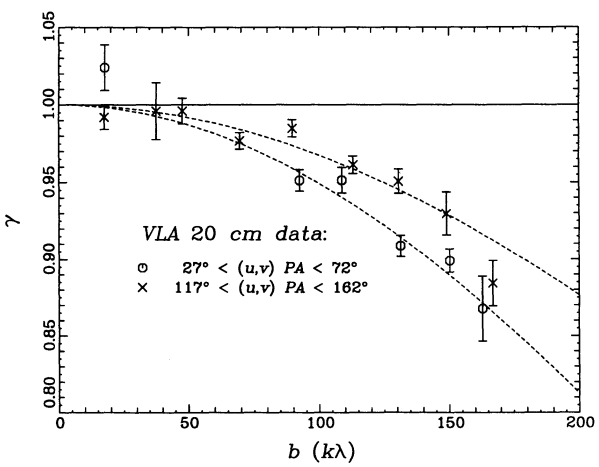

FIG. 6.—Interferometer visibility vs. baseline length in thousands of wavelengths for 20 cm wavelength VLA data along the major and minor axes of the scattering disk. Dashed lines denote the best-fit anisotropic scattering model to the combined VLA data sets.

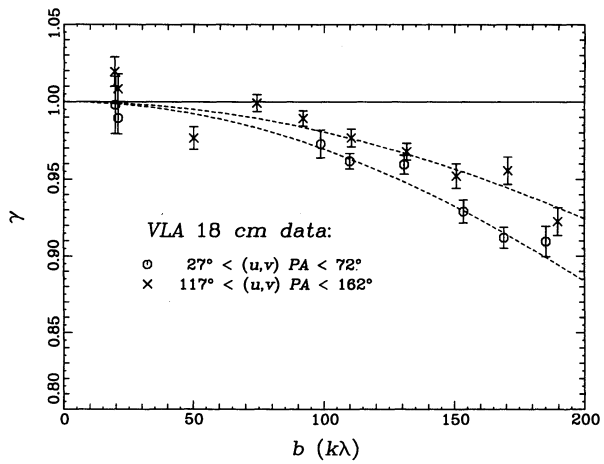

FIG. 7.—Interferometer visibility vs. baseline length in thousands of wavelengths for 18 cm wavelength VLA data along the major and minor axes of the scattering disk. Dashed lines denote the best-fit anisotropic scattering model to the combined VLA data sets.

the uncertainties, suggesting no significant change in the shape of the scattering disk in 4.3 yr. For completeness we note that θ_0 is 233.3 $\pm$ 3.3 mas in this model (for ν_0 = 1.5 GHz). The area of the scattering disk in this fit is consistent with that of the circular fit in our 1988 paper.

By binning the data according to b_s, we can show a one-dimensional presentation of the intrinsically two-dimensional VLA data. We add these binned data to Figure 5, the plot of visibility versus scaled baseline. For comparison we also plot a datum representative of the scattering measured in the 1.3 cm wavelength VLBI experiment of Molnar et al. (1988) by equating the area of their circular scattering model to a model with the ellipticity used here.

3. ANALYSIS OF THE COMBINED VLBI AND VLA DATA SETS

Given the lack of change in the shape of the scattering disk it is reasonable to fit the combined VLBI and VLA data sets. We will look for evidence of a break in the phase structure function. The value of β for the VLA data already provides marginal evidence for a break. A combined fit will make use of this information as well as the change in the amount of scattering (or the scattering size) with baseline, a comparison we have not yet made. We will first fit the data to an equation requiring β to be 4.0 for scaled baselines shorter than a break scale, l_b, with β a free parameter on longer baselines in order to establish in a relatively model-independent fashion the presence of a break. Then we will fit the data to a Kolomogorov power spectrum (which is generally used to fit pulsar scintillation data) with a cutoff at an inner scale, l_0.

3.1. *A Broken Power Law*

For a broken power law with a spectral break at an inner scale l_b, our expression for the model visibility becomes

$$\gamma(x, y) = \exp\left[-\ln 2\left(\frac{\pi\theta_0}{2\ln 2}\right)^{\beta-2}\left(\frac{b_s}{\lambda_0}\right)^2\left(\frac{\lambda}{\lambda_0}\right)^2\right] \quad \text{for} \quad b_s < l_b$$

$$= \exp\left[-\ln 2\left(\frac{\pi\theta_0}{2\ln 2}\right)^{\beta-2}\left(\frac{b_s}{\lambda_0}\right)^{\beta-2}\left(\frac{\lambda}{\lambda_0}\right)^2\right] \quad \text{for} \quad b_s > l_b\,. \quad (9)$$

This model provides a good fit to the data: a χ^2 of 273.8 for 275 degrees of freedom. We find l_b to be 29^{+17}_{-6} km (1 σ uncertainty). The uncertainty on l_b is not Gaussian distributed, so as this is the first ISS measurement of a break, we also compute the probabilities that we have failed to bound l_b on one side or the other. The probability is 0.10 that l_b is actually shorter than our shortest baseline (effectively 10 km). This is consistent with the only other observational result, that of Moran et al. (1990) cited above (although the inner scales in these two different lines of sight do not have to be the same). The probability is 3.4×10^{-4} that l_b is longer than our longest scaled baseline (170 km).

In Figure 8 we compare the model and the data by plotting as a function of b_s the quantity

$$G(\gamma, \lambda, b_s) \equiv \frac{-1}{4\pi^2 r_e^2 \mathscr{L}_\infty} \ln(\gamma) \lambda^{-2} b_s^{-5/3}, \quad (10)$$

which has units of $m^{-17/3}$, where r_e is the classical electron radius and $\mathscr{L}_\infty$ is a dimensionless factor defined in the next section. The wavelength factor in the definition of G allows data obtained at varying wavelengths all to be compared with the same model curve. The baseline factor makes the slope of the plot $\beta - 11/3$, thereby allowing changes in β in the range 11/3 to 4 to be relatively easily seen. The data are plotted with the same symbols used in Figure 7. We plot our best-fit model with a solid line. For reference we also mark the position of l_b along with its 1 σ uncertainty. Note that the 1.3 cm datum is not included in the fit as it was not derived in a fashion fully self-consistent with anisotropic scattering, but is plotted in Figure 8 for comparison.

The best-fit values for (β, ρ, χ, θ_0) in the combined fit are (3.92 ± 0.02, 1.275 ± 0.016, $51.^\circ5 \pm 1.^\circ4$, 225.6 ± 2.8 mas) for $\nu_0 = 1.5$ GHz. We find only two significant correlations among the parameters: β is negatively correlated with l_b and θ_0 is positively correlated with ρ. For baselines shorter than the inner scale length, our model corresponds to a Gaussian FWHM of the major axis of 235.0 mas, consistent with the value calculated for the VLA data alone.

3.2. *A Kolmogorov Spectrum with a Cutoff*

A Kolmogorov spectrum, which corresponds to a β of 11/3, has successfully been used to describe a wide variety of interstellar scintillation measurements. Spangler & Gwinn (1989) suggest that ISS measurements of β intermediate between 11/3 and 4 need not imply a non-Kolmogorov spectrum but rather may be an indication that the range of baselines used is near the inner scale, l_0, of the ISM. The shape of the cutoff at the inner scale is not known a priori, so we will try fitting both to a Gaussian cutoff (inner scale l_{0G}) and an exponential cutoff (inner scale l_{0E}). The corresponding spatial power spectra can be written as

$$Q_G(q_s) = C_N^2 q_s^{-11/3} \exp\left[-\left(\frac{q_s l_{0G}}{2\pi}\right)^2\right] \quad (11)$$

or

$$Q_E(q_s) = C_N^2 q_s^{-11/3} \exp\left[-\frac{q_s l_{0E}}{2\pi}\right]. \quad (12)$$

This corresponds to an interferometer visibility

$$\gamma = \exp\left[-4\pi^2 r_e^2 \lambda^2 C_N^2 L b_s^{5/3} \mathscr{L}(b_s)\right], \quad (13)$$

where L corresponds to the path length through the scattering region and

$$\mathscr{L}(b_s) \equiv C_N^{-2} b_s^{-5/3} \int_0^\infty dq[1 - J_0(qb_s)]qQ(q) \quad (14)$$

(see Cordes, Pidwerbetsky, & Lovelace 1986), where J_0 is a Bessel function. These equations assume a plane wave rather than a spherical wave, which is a reasonable approximation given the relative distances of the emitter and the scatterer discussed below.

For any cutoff, the limit of $\mathscr{L}(b_s)$ for b_s much greater than l_0, $\mathscr{L}_\infty$, is 1.118. In the limit of b_s much less than l_0

$$\mathscr{L}(b_s) = C\left(\frac{b_s}{l_0}\right)^{1/3} \mathscr{L}_\infty, \quad (15)$$

where C is 1.15 for the Gaussian cutoff and 1.11 for the exponential cutoff. Our earlier statement that β is effectively 4 for baselines much shorter than l_0 can now be shown by placing equation (15) into equation (13) and comparing with equation (6).

Using equation (13) in the definition of $G(\gamma, \lambda, b_s)$ (eq. [10]) we find

$$G(\gamma, \lambda, b_s) = \frac{\mathscr{L}(b_s)}{\mathscr{L}_\infty} C_N^2 L. \quad (16)$$

We can now interpret our log-log plot of G versus b_s: the absolute scale of G fixes the total scattering power $C_N^2 L$, the absolute scale of b_s fixes the inner scale l_0, and the detailed shape of the curve determines the cutoff function through the function $\mathscr{L}$. For baselines near l_0, our previous measure of total scattering power (the angular size of the scattering disk) is not well defined. In the asymptotic limits the FWHM scattering size is related to $C_N^2 L$ by

$$\theta = 3.2 \times 10^{-9} (C_N^2 L)^{3/5} \lambda^{11/5} \text{ mas} \quad \text{for } b_s \gg l_0$$

$$= 2.84 \times 10^{-7} C^{1/2} (C_N^2 L)^{1/2} \lambda^2 \left(\frac{l_0}{100 \text{ km}}\right)^{-1/6} \text{ mas} \quad \text{for } b_s \ll l_0, \quad (17)$$

where λ is in meters and $C_N^2 L$ is in $m^{-17/3}$.

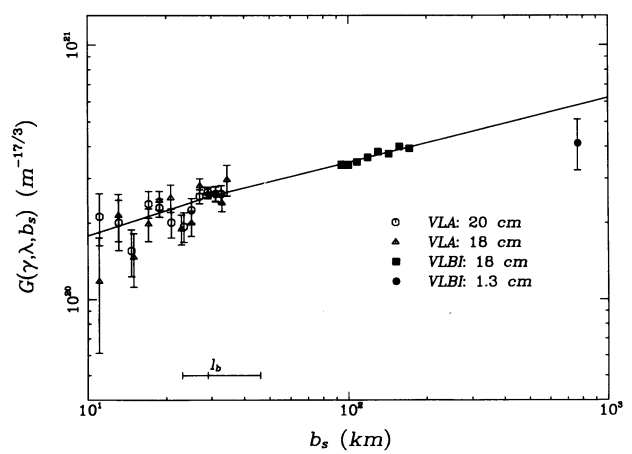

FIG. 8.—The observable $G(\gamma, \lambda, b_s)$ vs. baseline length, scaled for $(\rho, \chi) = (1.^\circ28, 51.^\circ5)$. The best-fit broken power-law phase structure function is marked with a solid line. The position of l_b along with its 1 σ uncertainty is marked at the bottom.

TABLE 1

FIT TO KOLMOGOROV SPECTRUM

Cutoff	Gaussian	Exponential
l_0 (km)	250^{+80}_{-50}	310^{+120}_{-70}
$C_N^2 L$ (10^{20} m$^{-17/3}$)	4.6 ± 0.4	5.1 ± 0.5
ρ	1.31 ± 0.02	1.30 ± 0.02
χ	$52.^{\circ}0 \pm 1.^{\circ}5$	$52.^{\circ}0 \pm 1.^{\circ}5$
$\theta_0(b_s \gg l_0)$ mas	231 ± 13	247 ± 15
$\theta_0(b_s \ll l_0)$ mas	224 ± 3	224 ± 3

Both the Gaussian and the exponential cutoffs provide good fits to the data, with χ^2 of 276.36 and 275.72, respectively, for 276 degrees of freedom. The best-fit parameter values and their 1 σ uncertainties are listed in Table 1.

In Figure 9 we again plot G versus b_s, this time using $(\rho, \chi) = (1.^{\circ}31, 52.^{\circ}0)$ to fix the scaling. The data are plotted with the same symbols used in Figure 7. The Gaussian cutoff model is given with a solid line, the exponential model with a dashed line. For reference we mark the best-fit values of l_{0G} and l_{0E}.

3.3. *Comparison with Previous Observations*

As has been noted at several points already, while previous measurements of scattering in Cyg X-3 have neither found anisotropy nor an inner scale length, they are also not of as high a quality as the present measurements and are not inconsistent with our model fit. The most sensitive previous measurements are the 408 MHz MERLIN data of Wilkinson et al. (1988), which they fit with a circular source of 2850 mas FWHM. They note the possibility that their data are anisotropic, finding an axial ratio of 1.07 ± 0.03, elongated north-south (the orientation of the radio jet), with no uncertainty in the orientation quoted. The difference between their axial ratio orientation and ours may be due to the intrinsic size of the source at that time. Their observation took place on 1986 January 3, just 89 days since the beginning of one of the largest flares recorded. Again using an expansion rate of ~ 10 mas day^{-1} we expect an intrinsic size of 850 mass at the date of their observations, enough to induce a change in the observed scattering disk.

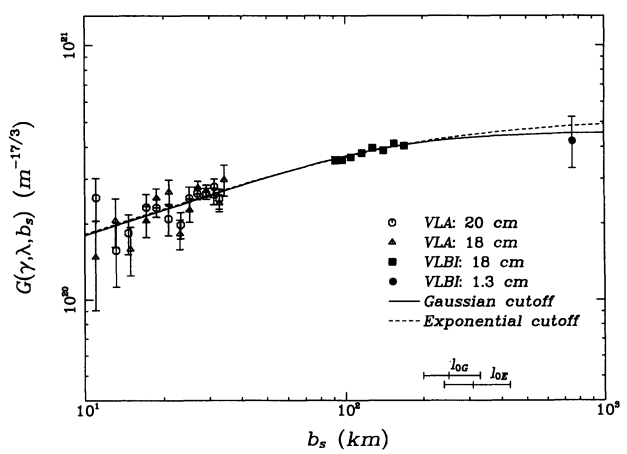

FIG. 9.—Observable $G(\gamma, \lambda, b_s)$ vs. baseline length, scaled for $(\rho, \chi) = (1.^{\circ}31, 52.^{\circ}0)$. The best-fit Kolmogorov turbulent spectrum with a Gaussian cutoff is marked with a solid line. The best-fit Kolmogorov spectrum with an exponential cutoff is marked with a dashed line. The positions of l_{0G} and l_{0E}, along with 1 σ uncertainties, are marked at the bottom.

Strom, van Paradijs, & van der Klis (1989) mapped Cyg X-3 at 4.8 GHz at Westerbork on 1987 October 14 and found faint lobes oriented north-south with a $\sim 6''$ separation. This matches well the expected separation for the giant flare, that began in 1985 December. Hence contrary to the interpretation of Strom et al. that these data indicate a new, time-independent component of the radio structure, we suggest they support the generality of the expanding jet model we have used above.

4. DISCUSSION

4.1. *Validity of Shallow Spectrum and Ensemble Average Assumptions*

Each of the expressions for interferometer visibility above (eqs. [9] and [13]) assumes a shallow spectrum ($\beta < 4$). Before we go on we must weigh the evidence for rejecting a steep spectrum ($\beta > 4$). Differing predictions are made for the amount of variation of the scattering with time, the overall shape of the phase structure function, and the presence of detailed structure in the phase structure function. We consider each in turn, following the theoretical development of Narayan & Goodman (1989).

For a steep spectrum we expect large changes in the size and shape of the scattering disk on the refractive time scale (the product of the scattering size and the distance to the scatterer divided by the velocity of the scattering medium across the line of sight). At 1.5 GHz this is ~ 200 yr (taking 2 kpc and 10 km s^{-1}), which is much greater than the 17 yr between our VLBI measurements and the first scattering measurements of Cyg X-3 by Anderson et al. (1972). Hence the observed upper limits on change in the scattering disk *cannot* distinguish between steep and shallow scattering. However we *can* take the long refractive time scale to further justify our combining data taken 4 yr apart in one fit.

For a steep spectrum we expect the ensemble average structure function to depend on baseline squared for short baselines, with a break near the *outer* scale, L_0. But for refractive effects to be important, L_0 must be greater than the refractive scale ($\sim 7 \times 10^{10}$ km), so the break cannot be a measure of the outer scale.

Our expressions further assume an ensemble average, which is not strictly true because our integration time is much less than the refractive time (Narayan & Goodman 1989). As formulated by Narayan & Goodman, the deviation from an ensemble average is only significant for baselines greater than the diffractive scale (the scale at which the phase structure function is unity). On average the steep spectrum will deviate more sharply, in the sense of the visibilities dropping off too slowly as a function of baseline, whereas the shallow spectrum will not show noticeable deviation for baselines less than several diffractive scales. The visibilities will also vary on the refractive time scale. In a specific realization (steep or shallow) one also expects to see structure in the deviation with baseline. Our longest baselines are approximately twice the diffractive scale, and the data are consistent with an ensemble average model. For a steep spectrum this consistency is permitted, but must be interpreted as a coincidence as a typical realization would be far from the ensemble average. For a shallow spectrum by contrast this consistency is required for our baseline range.

4.2. *Inner Scale of the Interstellar Medium*

Having demonstrated the plausibility of our assumptions, we interpret the observed break in the phase structure function

as the inner scale of the turbulent power spectrum. Our value for l_0 is 300 km with an uncertainty of $\sim 50\%$, arising in equal parts from the quality of the data and the uncertainty as to what cutoff function to use. In the light of this datum we now consider which phase of the ISM contains the scattering plasma and what mechanism fixes the inner scale.

Cordes, Weisberg, & Boriakoff (1985) suggest a two-component model for the electron density fluctuations in the Galaxy consisting of a highly scattering component with low filling factor and scale height and a moderately scattering component with a large filling factor and scale height. The high inferred value of $C_N^2 L$ for the scattering screen and the low Galactic latitude (0°.7) of Cyg X-3 favor the former component.

Anantharamaiah & Narayan (1988) suggest the outer envelope of H II regions can account statistically for the amount of scattering seen in heavily scattered sources at low Galactic latitude and longitude. Spangler & Gwinn (1989) point out that the expected inner scale in such regions is ~ 200 km (set by the ion Larmor radius), in good agreement with our observed value. They expect the inner scale in the warm and coronal components of the ISM to be 450 and 3800 km, respectively (set by the ion inertial length). The former is also consistent with our value, but the latter is ruled out completely.

Spangler & Gwinn (1989) also plot observed values of β (in the sense of eq. [6]) for six heavily scattered sources versus the baseline of the measurement. They compare these data to a Kolmogorov spectrum with an exponential cutoff, concluding the data are consistent with a single inner scale of a few hundred kilometers, consistent with our value for Cyg X-3. These results are complementary in the following sense. Given the small number of data, Spangler and Gwinn's plot is also consistent with a random variation in β with line of sight (and no cutoff) with a coincidental correlation. But the Cyg X-3 data show that for at least one line of sight β does vary with baseline in the expected manner. Given this point, Spangler & Gwinn's plot shows the specific value of the inner scale may be general to different lines of sight.

By contrast Coles et al. (1987) suggest an inner scale of $\sim 10^6$ km for the moderately scattering component in order to account for the intensity of refractive scintillation in these sources. This inner scale is inconsistent with our measured value, but there is no particular reason the inner scale should be the same in both scattering components of the ISM.

4.3. *The Line of Sight to Cyg X-3*

In this section we want to summarize and interpret what is known about the line of sight to Cyg X-3, in particular determining the properties of any H II regions. We will identify the H II region DR 11 as the likely host plasma for the scattering of Cyg X-3.

4.3.1. *Overview*

Cyg X-3 is at Galactic longitude 79°.8 and is at least 10 kpc (Dickey 1983). Out to a distance of ~ 4 kpc the line of sight traverses the local spiral arm (the Orion arm) lengthwise; further out it crosses the two Perseus arms (see the review by Bochkarev & Sitnik 1985). We indicate these features, and others discussed below, in a map of the Galaxy as viewed from above in Figure 10. A variety of features are seen in projection within the local arm. The line of sight enters the Great Rift at a distance of about 1 kpc, and crosses the southern edge of the extremely massive and luminous Cyg OB2 association at a

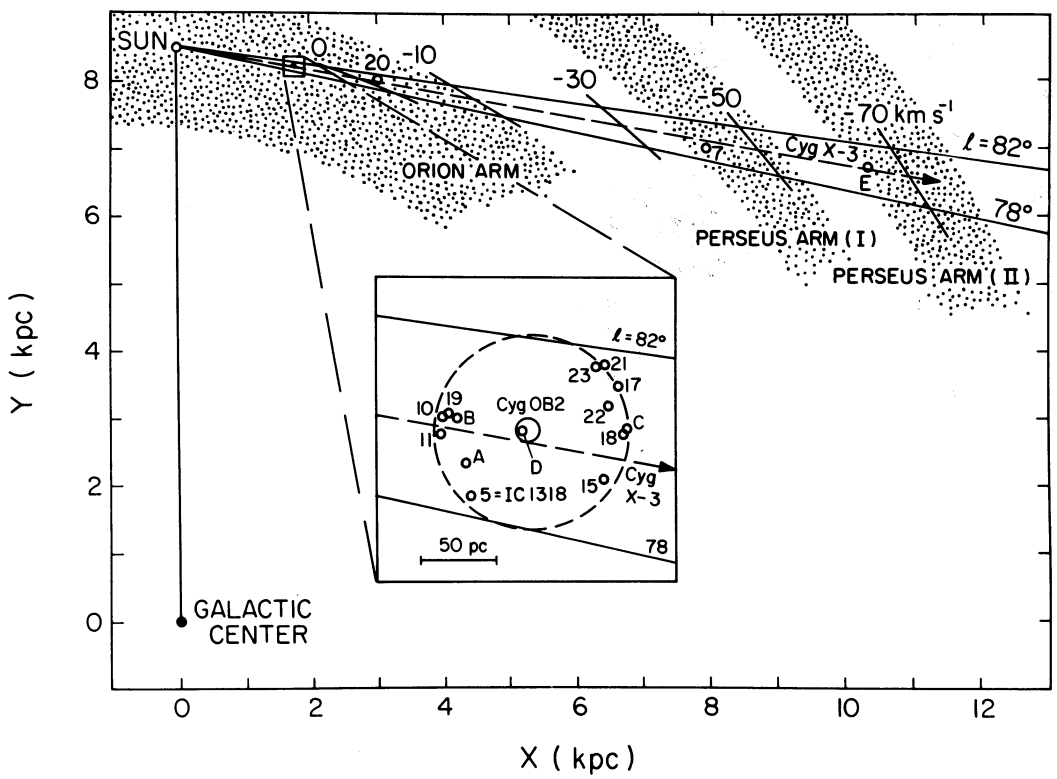

FIG. 10.—Schematic map of the Galaxy as viewed from above, with an inset enlarging the area around Cyg OB2. We mark the locations of the H II regions listed in Table 2 as deduced in the text. We also indicate the line of sight to Cyg X-3.

distance of 1.8 ± 0.2 kpc (Humphreys 1978). The line of sight also likely crosses two or more molecular clouds within the local arm (Piepenbrink & Wendker 1988).

4.3.2. *The Cygnus X Radio Source: An Expanding Shell around Cyg OB2*

Cyg X-3 is embedded in the Cygnus X radio emission region, an unusually dense group of H II regions which we wish to consider in some detail. We reproduce in Figure 11*a* a radio map of the central portion of Cygnus X using data from the 4.85 GHz survey of Condon, Broderick, & Seielstad (1989). For comparison we reproduce in Figure 11*b* the E plate of the Palomar Sky Survey (PSS). Piepenbrink & Wendker (1988) measured recombination line LSR velocities to 16 H II regions within 2° of Cyg OB2, which we list in Table 2 along with their Galactic coordinates. (We average together multiple observations made in different locations of the same source.) We list either the DR number designation (for those sources listed in Downes & Rinehart 1966) or assign a letter designation. We also add an entry for DR 11 using data from the recombination line survey of Landecker (1984). We obtain an indication of the reliability of these velocities by noting that they agree with those in the survey of Lockman (1989) to within 3 km s^{-1} or better.

Huchtmeier & Wendker (1977) discuss the need to have some H II region associated with Cyg OB2 to reprocess the enormous Lyman continuum produced there, but they fail to find any compact H II regions near Cyg OB2. Cash et al. (1980) suggest the entire Cygnus X region, along with a ring of optical emission nebulae and of diffuse X-ray emission, constitutes a superbubble around Cyg OB2 of diameter 13°. Bochkarev & Sitnik (1985) show the various elements of the proposed superbubble are not physically related, and suggest that the Cygnus X region is a chance superposition of physically unrelated sources seen together in projection.

TABLE 2

H II REGIONS WITH 2° OF Cyg OB2

DR (1)	l (2)	b (3)	v (km s^{-1}) (4)	$v - v_{model}$ (5)
5.....	78°51	1°22	−6.7	−0.6
10.....	80.05	1.53	−10.5	−0.0
11.....	79.67	1.30	−11.3	−0.9
15.....	79.31	0.28	6.	−1.4
17.....	81.30	1.16	10.3	3.1
18.....	80.36	0.45	7.	−1.7
19.....	80.10	0.09	−3.2	6.9
21.....	81.68	0.54	−1.0	−6.5
22.....	80.86	−0.25	3.3	−3.2
23.....	81.61	0.01	−0.4	−4.9
A.....	79.15	−0.26	−2.	5.2
B.....	80.03	2.11	−4.8	4.1
C.....	80.45	1.05	9.	0.1
7.....	79.30	1.30	−40.8	−31.1
20.....	80.88	0.42	−1.5	8.6
D.....	80.20	0.80	−1.	−10.0
E.....	80.35	0.73	−64.6	−53.7

Landecker (1984) suggests the cluster of H II regions near DR 21 and the cluster near DR 5 (= IC1318) may be related to Cyg OB2, one behind and the other in front. Establishing the distances to verify this is difficult. Radial velocity due to Galactic rotation can be used to distinguish between the three spiral arms (see Fig. 10). This method places DR 7 in Perseus arm (I) and source E in Perseus arm (II). However, the range of rotation velocities within the local arm, 25 km s^{-1} (+5 to −20 km

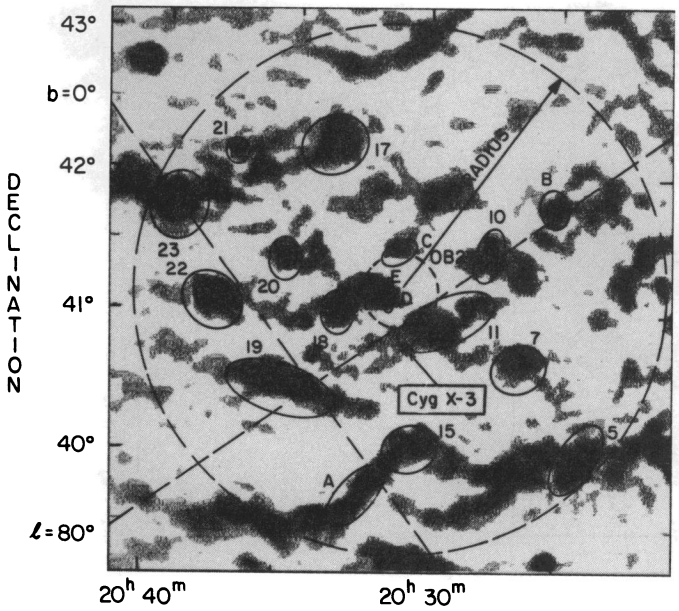

FIG. 11*a*

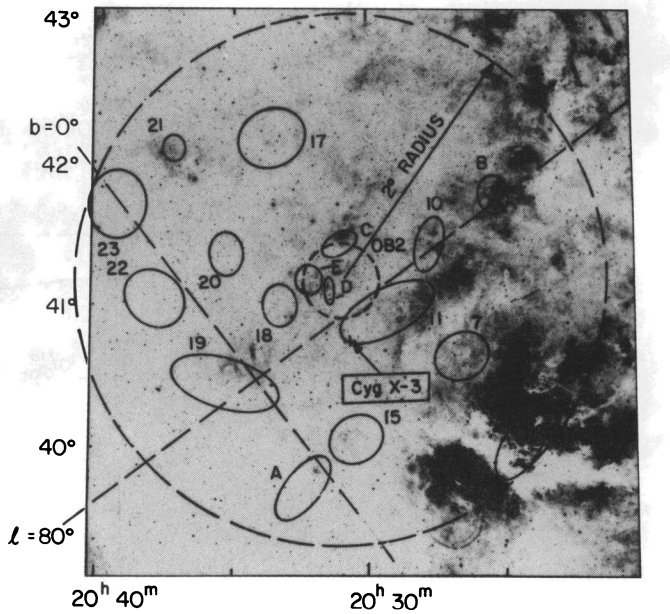

FIG. 11*b*

FIG. 11.—(*a*) Radiograph of the central portion of Cygnus X at 4.85 GHz from the survey of Condon et al. (1989). We set to zero areas on the map for which no data were obtained because of problems with sidelobes. Comparison with the map of Wendker (1984) shows that these are in fact areas of low intensity. We mark the positions of Cyg X-3, Cyg OB2, and the H II regions listed in Table 2. We also mark a circle of 2° radius centered on Cyg OB2. (*b*) the same portion of sky from the PSS E plate.

s^{-1}), is not much greater than the range arising from random peculiar velocities, and hence cannot be used to determine distances of individual sources. Visual extinction in this direction varies greatly over small angular scales, limiting the usefulness of stellar extinction curves for distance determination. Landecker notes the small range of velocities for the H II regions within each of the two clusters as evidence for physical relationship.

Building on Landecker's interpretation, we suggest that a broad range of observations may be accounted for under the hypothesis that there is a shell of radius 2° (60 pc) centered on Cyg OB2 with center velocity -1 km s^{-1} and expanding at ~ 10 km s^{-1}. Münch (1957) and Philips, Welsh, & Pettini (1984) give evidence for expanding gas shells with similar velocities around other OB associations. In column (5) of Table 2, we list the residuals of the observed velocities with respect to this model. This model would resolve the question of the missing H II region. Excluding DR 7 and source E, which are known to be background sources, and sources DR 20 and source D, which we discuss below, this model reduces the rms scatter of the 13 remaining velocities from 7.1 to 3.9 km s^{-1}, which is not very much greater than the observational uncertainties. The size, distance, and velocity imply an age of 6×10^6 yr (or less if there is deceleration), which is consistent with the age of Cyg OB2.

The model does not account well for DR 20, which has a velocity inconsistent with either the front or back of the shell. The velocity corresponds to a Galactic rotation distance behind Cyg OB2, so it may be a third unrelated background source. Alternatively, it may be at the back of the shell near DR 21, with a unusual velocity due to local deviations from our idealized expanding sphere.

The only other H II region that does not fit the picture well is source D. It is projected onto the center of Cyg OB2 on top of star No. 8, a trapezium of four O stars behind 5 mag of extinction (Schulte 1958). As it has the center velocity for Cyg OB2 and extinction consistent with star No. 8, we suggest it is physically associated.

Given the subjectivity of interpreting a complex set of data, we regard our expanding shell hypothesis as promising, accounting for a broad range of data with relatively few parameters, but not proven by the velocity data alone. A more comprehensive development of this idea will be published in a separate article (Molnar & Halas 1993).

4.3.3. H II *Regions toward Cyg X-3*

The line of sight to Cyg X-3 passes through the outer portions of DR 11, which we place on the near side of the expanding shell. The detailed structure of this region correlates well between the 4.8 GHz continuum map of Wendker (1984) and the Hα emission seen on the PSS E plate or the Hα plate of Dickel & Wendker (1977). Dickel & Wendker (1978) find an extinction of 4 ± 0.5 mag, consistent with the front of the shell. Near the position of Cyg X-3, Landecker (1984) measured an H166α recombination line with width and centroid consistent with a blend of the lines of DR 11 and DR 15. DR 15 is centered 40′ south of Cyg X-3 and has velocity and extinction consistent with the back of the shell. Given the different extinction, we suggest that DR 15 is not seen directly along the line of sight to Cyg X-3, but rather was also present at the edge of the 36′ beam of the H166α measurement.

From the 4.8 GHz map (Wendker 1984) we estimate the emission measure, EM, toward Cyg X-3 to be ~ 6000 cm^{-6} pc for an assumed effective temperature of 6000 K. Spangler & Reynolds (1990) show that for scattering by H II regions with strong turbulence and similar outer scales, the ratio $C_N^2 L/\mathrm{EM}$ should be constant. The value of this ratio for Cyg X-3 is similar to that found by Spangler & Reynolds for several other highly scattered sources, again consistent with the hypothesis that the H II region DR 11 is the host plasma for the scattering.

4.4. *Interpretation of Anisotropic Turbulence*

The second major observational result of this project is the observation of 30% anisotropy in the scattering disk. This is the first unambiguous indication of anisotropic scattering in the ISM both because of the high statistical significance (3.3 σ in the VLBI data set and greater than 5 σ in each of the VLA data sets) and because of the clear distinction between the orientation of the scattering disk ($52\overset{\circ}{.}0 \pm 1\overset{\circ}{.}5$) and that of the intrinsic structure ($\sim 0°$). Three other possible cases have been cited in the literature. Gwinn at al. (1988) find an axial ratio of 1.7 for PSR 1933+16, but as the anisotropy depends entirely on the poorly calibrated Arecibo baseline they state this only as an upper limit. Jauncey et al. (1989) find an axial ratio of 1.9 ± 0.4 for Sgr A* at 3.6 cm. As this has been measured at only one wavelength and over a limited range of baselines, it cannot yet be determined whether the anisotropy is intrinsic source structure or a result of scattering. Finally, Spangler & Cordes (1988) find an axial ratio of 1.4 for 2013+37 with a high SNR. However the orientation they find, $12° \pm 2°$, is coincident with the orientation of the intrinsic structure, 14°.

There are several types of mechanisms that can produce anisotropy. Refractive effects are discussed by Spangler & Cordes (1988). The results of our model fitting did not suggest refraction, but it remains possible that larger spatial scales than we have sampled are refractive. A second possibility is that the ISM may have irregular structure on the size scale of the diffraction disk. This angular structure would be independent of wavelength, and so could be distinguished from wavelength-dependent diffraction. This does not apply to Cyg X-3 if the scattering occurs in the H II regions, which dominate the 20 cm wavelength interferometer visibilities in the D-array of the VLA, but are completely resolved in the A-array. The remaining possibility is anisotropic diffraction, which we consider in more detail.

Romani, Narayan, & Blandford (1986) find that random fluctuations in an isotropic, shallow spectrum can yield an axial ratio of ~ 1.1, but our observed value of 1.31 ± 0.02 seems too large to be accounted for by this model.

The uniform component of the interstellar magnetic field provides a natural source for anisotropy. Higdon's (1984) model of anisotropic magnetogasdynamic turbulence predicts the scattering disk should be perpendicular to the magnetic field. Recent observations by Armstrong et al. (1990) show this to be the case for the near-Sun solar wind. Alternatively, Spangler et al. (1986) and Spangler, Fey, & Cordes (1987) discuss the possibility of Alfvén waves produced in shocks which in turn produce density fluctuations. In this picture the scattering disk should be elongated parallel to the magnetic field.

It may be possible to determine the orientation of the magnetic field in DR 11 by comparing the interstellar polarization of starlight toward stars just in front of and just behind it. Finding an orientation either parallel or perpendicular to the radio-scattering disk would further secure the identification of this H II region with the scattering medium, as well as distinguish uniquely between the two turbulence models.

The position angle of interstellar polarization for Cyg X-3 itself ($-2\overset{\circ}{.}8 \pm 1\overset{\circ}{.}2$, Molnar & Jones 1993) is neither parallel nor perpendicular to the scattering disk. However the extinction to Cyg X-3 ($A_V \sim 17$, Molnar et al. 1993) is much greater than that of DR 11, so the polarization is dominated by the magnetic field behind DR 11. Other existing observations (Hiltner 1956) are too sparsely sampled to be conclusive. We have begun a program of measuring interstellar polarization of stars near this line of sight to fix the orientation of the magnetic field. For O and B stars at the distance of Cyg OB2 we expect apparent visual magnitudes from 9 to 12, depending on spectral type, and visual polarizations of about 5%.

Finally, we note that for anisotropic turbulence the inner scale may well be different along and across the magnetic field. Indeed our parameter l_0 applies along the major axis of the scattering disk, and our equations implicitly assume the inner scale is ρl_0 along the minor axis. While our data are consistent with this model, better sampling in the (u, v) plane will be needed to confirm this. We encourage the development of the theory on this point as it will be much easier to establish the ratio of inner scales than the absolute value (due to uncertainty in the cutoff function).

4.5. *Further Observations*

While the present data set is noteworthy for its accuracy, increased sensitivity or more complete (u, v) coverage, such as will be possible with the complete VLBA, can significantly improve the data in the entire range from 10 to 1000 km. On longer and shorter baselines the fundamental limiting factors are intrinsic source structure and large scale confusion sources, respectively.

Finally, as most of the Cygnus X region (which covers some 20 deg^2) has emission measure greater than or equal to that of Cyg X-3, a scattering study of extragalactic sources in this region could further establish the connection between heavy scattering and H II regions, as well as provide more examples of anisotropic scattering. We have surveyed the region with the VLA, finding 16 new sources with flux density greater than 40 mJy at 20 cm wavelength and no evidence of large-scale structure. We plan a detailed study of these sources with the VLBA.

We thank Elizabeth Waltman for timely notification of the June flare and Barry Clark and Joan Wrobel at NRAO for the prompt scheduling of the VLA and the VLBA that was essential to obtaining this unique data set. We thank Steve Unwin for prompt processing of the data with the Caltech correlator. We thank David Cohen for assistance in the development of the calibration software. Finally we acknowledge fruitful discussions with Steve Spangler and Ramesh Narayan on models of interstellar turbulence. This work was supported in part by NASA grant NAGW-831.

REFERENCES

Anantharamiah, K. R., & Narayan, R. 1988, in Radio Wave Scattering in the Interstellar Medium, ed. J. Cordes, B. Rickett, & D. Backer (AIP Conf. Proc. 174), 185
Anderson, B., Conway, R. G., Davis, R. J., Peckham, R. J., Richards, P. J., Spencer, R. E., & Wilkinson, P. N. 1972, Nature Phys. Sci., 239, 117
Armstrong, J. W., Coles, W. A., Kojima, M., & Rickett, B. J. 1990, ApJ, 358, 685
Avni, Y. 1976, ApJ, 210, 642
Bochkarev, N. G., & Sitnik, T. G. 1985, Ap&SS, 108, 237
Cash, W., Charles, P., Bowyer, S., Walter, F., Garmire, G., & Riegler, G. 1980, ApJ, 238, L71
Coles, W. A., Frehlich, R. G., Rickett, B. J., & Codona, J. L. 1987, ApJ, 315, 666
Condon, J. J., Broderick, J. J., & Seielstad, G. A. 1989, AJ, 97, 1064
Cordes, J. M., Pidwerbetsky, A., & Lovelace, R. V. E. 1986, ApJ, 310, 737
Cordes, J. M., Weisberg, J. M., & Boriakoff, V. 1985, ApJ, 288, 221
Dickel, J. R., & Wendker, H. J. 1977, A&AS, 29, 209
———. 1978, A&A, 66, 289
Dickey, J. M. 1983, ApJ, 273, L71
Downes, D., & Rinehart, R. 1966, ApJ, 144, 937
Gwinn, C. R., Cordes, J. M., Bartel, N., Wolszczan, A., & Mutel, R. L. 1988, ApJ, 334, L13
Higdon, J. C. 1984, ApJ, 285, 109
Hiltner, W. A. 1956, ApJS, 2, 389
Huchtmeier, W. K., & Wendker, H. J. 1977, A&A, 58, 197
Humphreys, R. M. 1978, ApJS, 38, 309
Jauncey, D. L., et al. 1989, AJ, 98, 44
Johnston, K. J., et al. 1986, ApJ, 309, 707
Landecker, T. L. 1984, AJ, 89, 95
Lockman, F. J. 1989, ApJS, 71, 469
Molnar, L. A. 1988, ApJ, 331, L25
Molnar, L. A., & Halas, C. 1993, in preparation
Molnar, L. A., & Jones, T. J. 1993, in preparation
Molnar, L. A., Reid, M. J., & Grindlay, J. E. 1984, Nature, 310, 662
———. 1985, in Radio Stars, ed. R. M. Hjellming & D. M. Gibson, Astrophysics and Space Science Series (Dordrecht: Reidel), 329
———. 1988, ApJ, 331, 494
Molnar, L. A., Reid, M. J., Grindlay, J. E., & Willmer, S. P. 1993, in preparation
Moran, J. M., Rodríguez, L. F., Greene, B., & Backer, D. C. 1990, ApJ, 348, 147
Münch, G. 1957, ApJ, 125, 42
Mutel, R. L., & Lestrade, J. F. 1990, ApJ, 349, L47
Napier, P. J., Thompson, A. R., & Ekers, R. D. 1983, Proc. IEEE, 71, 1295
Narayan, R., & Goodman, J. 1989, MNRAS, 238, 963
Narayan, R., & Hubbard, W. B. 1988, ApJ, 325, 503
Philips, A. P., Welsh, B. Y., & Pettini, M. 1984, MNRAS, 206, 55
Piepenbrink, A., & Wendker, H. J. 1988, A&A, 191, 313
Romani, R. W., Narayan, R. D., & Blandford, R. D. 1986, MNRAS, 220, 19
Schulte, D. H. 1958, ApJ, 128, 41
Spangler, S. R., & Cordes, J. M. 1988, ApJ, 332, 346
Spangler, S. R., Fey, A. L., & Cordes, J. M. 1987, ApJ, 322, 909
Spangler, S. R., & Gwinn, C. R. 1989, ApJ, 353, L29
Spangler, S. R., Mutel, R. L., Benson, J. M., & Cordes, J. M. 1986, ApJ, 301, 312
Spangler, S. R., & Reynolds, R. J. 1990, ApJ, 361, 116
Strom, R. G., van Paradijs, J., & van der Klis, M. 1989, Nature, 337, 234
Voelcker, K., & Elsässer, H. 1973, in IAU Symp. 52, Interstellar Dust and Related Topics, ed. J. M. Greenberg & H. C. Van de Hulst (Dordrecht: Reidel), 529
Waltman, E. B., Fiedler, R. L., & Johnston, K. J. 1989, IAU Circ., No. 4798
Wendker, H. J. 1984, A&AS, 58, 291
Wilkinson, P. N., Spencer, R. E., & Nelson, R. F. 1988, in IAU Symp. 129, The Impact of VLBI on Astrophysics and Geophysics, ed. M. J. Reid & J. M. Moran (Dordrecht: Reidel), 305